A&A 600, A108 (2017)
DOI: 10.1051/0004-6361/201629615

Astronomy & Astrophysics

Radiative data for highly excited $3d^8 4d$ levels in Ni II from laboratory measurements and atomic calculations

H. Hartman[1,2], L. Engström[3], H. Lundberg[3], H. Nilsson[2,3], P. Quinet[4,5], V. Fivet[4], P. Palmeri[4], G. Malcheva[6], and K. Blagoev[6]

[1] Materials Science and Applied Mathematics, Malmö University, 20506 Malmö, Sweden
e-mail: Henrik.Hartman@mah.se
[2] Lund Observatory, Lund University, Box 43, 221 00 Lund, Sweden
[3] Department of Physics, Lund University, Box 118, 221 00 Lund, Sweden
[4] Physique Atomique et Astrophysique, Université de Mons, 7000 Mons, Belgium
[5] IPNAS, Université de Liège, 4000 Liège, Belgium
[6] Institute of Solid State Physics, Bulgarian Academy of Sciences, 72 Tzarigradsko Chaussee, 1784 Sofia, Bulgaria

Received 30 August 2016 / Accepted 6 December 2016

ABSTRACT

Aims. This work reports new experimental radiative lifetimes and calculated oscillator strengths for transitions from $3d^8 4d$ levels of astrophysical interest in singly ionized nickel.
Methods. Radiative lifetimes of seven high-lying levels of even parity in Ni II (98 400−100 600 cm^{-1}) have been measured using the time-resolved laser-induced fluorescence method. Two-step photon excitation of ions produced by laser ablation has been utilized to populate the levels. Theoretical calculations of the radiative lifetimes of the measured levels and transition probabilities from these levels are reported. The calculations have been performed using a pseudo-relativistic Hartree-Fock method, taking into account core polarization effects.
Results. A new set of transition probabilities and oscillator strengths has been deduced for 477 Ni II transitions of astrophysical interest in the spectral range 194−520 nm depopulating even parity $3d^8 4d$ levels. The new calculated *gf*-values are, on the average, about 20% higher than a previous calculation and yield lifetimes within 5% of the experimental values.

Key words. atomic data – methods: laboratory: atomic – techniques: spectroscopic

1. Introduction

The final stage of exothermal element production in massive stars is the iron-group elements, with nickel itself having the maximum binding energy per nucleon closely followed by iron. Higher *Z* elements are produced by subsequent neutron capture. Nickel is therefore one of the most abundant iron-peak elements in cosmic objects. In addition, Nickel shows a line-rich spectrum due to its complex atomic structure and the lines appear in a variety of objects, from the interstellar medium and stars to the solar corona and supernova explosions. Nuclear statistical equilibrium models predict that iron and nickel are produced in high-temperature environments, i.e. explosive nucleosynthesis (Nadyozhin 2003), such as supernovae type Ia, where a white dwarf ignites, or supernovae type II, where the core of a massive star collapses into a neutron star (Stritzinger et al. 2006). The dominating product of these events is ^{56}Ni, which is distributed to the surrounding gas during the outburst. Abundance determinations of nickel in stars serve as important constraints of stellar evolution and supernova explosion models. The current challenges for accurate elemental abundances are the development of 3D-model atmospheres and non-LTE modeling (Wongwathanarat et al. 2011; Lind et al. 2012). Atomic data for levels of different excitation energies are important for this development. For example, in metal-rich stellar photospheres, transitions from low excitation states with a high population can be saturated whereas those from the less populated highly excited states are more likely to be optically thin. The present investigation of Ni II is part of an ongoing effort to provide such data for the second spectra of selected iron-group elements: Ti II (Lundberg et al. 2016), Cr II (Engström et al. 2014), Fe II (Hartman et al. 2015) and Co II (Quinet et al. 2016).

There are two papers in the literature on experimental determination of radiative lifetimes in Ni II. Lawler & Salih (1987) used the time-resolved laser-induced fluorescence (TR-LIF) method on a slow Ni^+ beam from a hollow-cathode source. Radiative lifetimes of 12 odd-parity levels of Ni II in the energy range from 51 550 to 57 080 cm^{-1} are reported in that paper. Later, Fedchak & Lawler (1999) improved the experimental set-up, confirmed and extended the previous results to a total of 18 experimental lifetimes and reported transition probabilities for 59 lines in the VUV and UV spectrum of Ni^+, Ni II.

In the present work, we have measured lifetimes for seven even-parity levels in the energy range 98 400 to 100 600 cm^{-1}. The lifetimes are measured using the TR-LIF method, and the high-lying states are populated using two-step photon excitation of ions produced by laser ablation. Furthermore, we report theoretical lifetimes obtained with a pseudo-relativistic Hartree-Fock method in good agreement with the experimental results, and calculated transition probabilities for 477 lines depopulating highly excited levels belonging to the even-parity $3d^8 4d$ configuration in singly ionized nickel.

Table 1. Levels measured in the $3d^8(^3F)4d$ configuration of Ni II and the corresponding excitation schemes.

Final level	First step excitation[a] Start level E^b (cm^{-1})	Intermediate E^b (cm^{-1})	λ_{air} (nm)	Second step excitation Final level E^b (cm^{-1})	λ_{air} (nm)	Scheme[c]	Detection Lower level E^b (cm^{-1})	λ_{air} (nm)
$^4D_{7/2}$	8393.9	54 557.0	216.6	98 467.25	227.7	$3\omega + S$	51 557.8	213[d]
$^4H_{13/2}$	8393.9	53 496.5	221.6	98 822.55	220.6	3ω	53 496.5	221[e]
$^4G_{11/2}$	8393.9	53 496.5	221.6	99 132.78	219.0	3ω	54 557.0	224[d]
$^4F_{9/2}$	8393.9	53 496.5	221.6	99 154.81	218.9	3ω	51 557.8	210, 224[d]
		54 557.0	216.6		224.1	$3\omega + S$	54 557.0	210
$^4D_{5/2}$	9330.0	55 417.8	216.9	99 559.33	226.5	3ω	52 738.4	214[d]
$^4H_{11/2}$	9330.0	55 299.6	217.5	100 309.29	222.1	3ω	55 299.6	222[d]
$^4G_{9/2}$	8393.9	54 557.0	216.6	100 619.26	217.0	3ω	56 371.4	226

Notes. [a] For all measured levels, the first excitation step used the frequency tripled (3ω) output from the dye laser; [b] Shenstone (1970); [c] S imply one added Stokes component of 4153 cm^{-1}; [d] corrected for fluorescence background from the intermediate level; [e] corrected for scattered light from both lasers, see also Fig. 2.

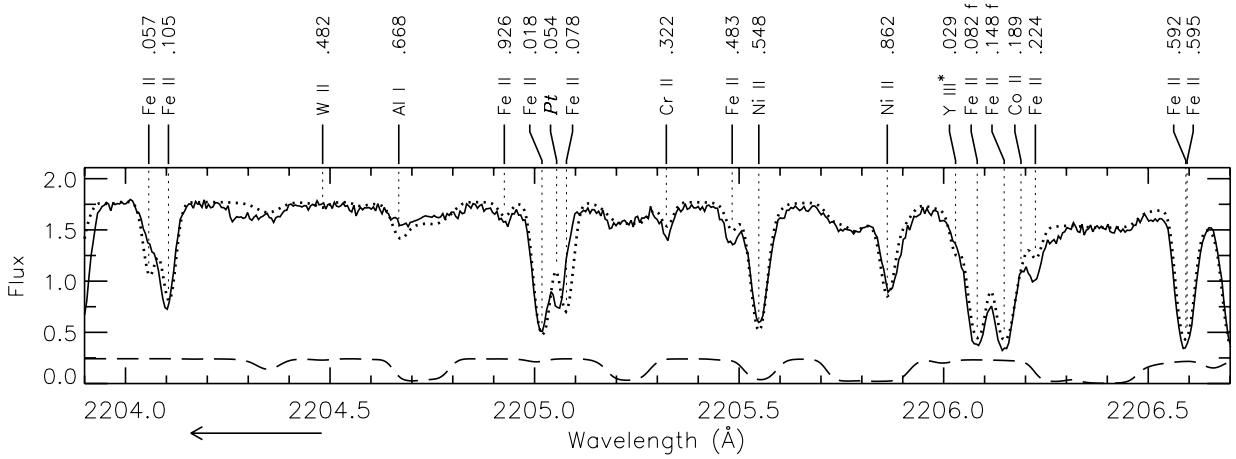

Fig. 1. HST/GHRS spectrum of Chi Lupi in the region around 2205 Å, showing the prominent Ni II lines at 2205.548 and 2205.862 Å studied in the present work. The solid line is the observed spectrum and the dashed line is the synthetic spectrum. Courtesy of Brandt et al. (1999) and reproduced by permission of the AAS.

The lines studied in the present work appear strong in spectra of hot stars, such as the B9.5V type HgMn star Chi Lupi A (Brandt et al. 1999), where the lines form prominent absorption features despite their higher excitation. As an example, a spectral segment of Chi Lupi from the HST/GHRS atlas is presented in Fig. 1. In addition, the Ni II lines are identified in several cooler template stars, e.g. the solar type star α Cen A (spectral type G2 V) and Arcturus (K1.5 III) as reported by Hinkle et al. (2005). In the linelists of these stars, several Ni II lines are presented without multiplet number, indicating that they are of too high excitation to be listed in the multiplet table by Moore (1959). All the Ni II lines in the 2000–3000 Å region without multiplet number are included in our study.

2. Experiment

The ground term in Ni II is [Ar] $3d^9\ ^2D$, but as a starting point in the excitation schemes we used the $J = 9/2$ and 7/2 levels in the second lowest term of even parity, $3d^8(^3F)4s\ ^4F$, at 8394 and 9330 cm^{-1}, respectively (Shenstone 1970). These levels were populated directly in the plasma produced by the ablation laser. The first tuneable laser excited the intermediate, odd parity, levels in the $3d^84p$ configuration around 55 000 cm^{-1}, from where the final, even parity, levels in $3d^84d$ around 100 000 cm^{-1} were reached with the second tuneable laser. The excitation and detection channels used in this work are given in Table 1.

The experimental set-up for two-step excitations at the Lund High Power Laser Facility has recently been described by Lundberg et al. (2016), and for an overview we refer to Fig. 1 in that paper. Here we only give the most important details. Ni^+ ions in the $3d^8(^3F)4s\ ^4F$ term were created by focusing 532 nm, 10 ns long, laser pulses onto a rotating nickel target placed in a vacuum chamber with a pressure of about 10^{-4} mbar. The two short wavelength excitation laser beams entered the vacuum chamber at a small relative angle and were focused on the expanding plasma plume about 5 mm above the target. All lasers operated at 10 Hz and were synchronized by a delay generator. The time resolved fluorescence from the excited states (both intermediate and final) was detected at right angles to the lasers by a 1/8 m grating monochromator, with its 0.28 mm wide entrance slit oriented parallel to the excitation laser beams and perpendicular to the ablation laser. The dispersed light was registered by a fast micro-channel-plate photomultiplier tube (Hamamatsu R3809U) and digitized by a Tektronix DPO 7254 oscilloscope. A second channel on the oscilloscope simultaneously registered the excitation pulse shape, as detected by a fast photo diode. The

Table 2. Radiative lifetimes (in ns) for selected energy levels belonging to the $3d^8(^3F)4d$ configuration of Ni II.

Level	Energy[a] (cm^{-1})	Experiment This work	Calculations This work	Kurucz[b]
$^4D_{7/2}$	98467.25	1.28 ± 0.1	1.30	1.43
$^4H_{13/2}$	98822.55	1.25 ± 0.1	1.32	1.41
$^4G_{11/2}$	99132.78	1.32 ± 0.1	1.34	1.43
$^4F_{9/2}$	99154.81	1.20 ± 0.1	1.29	1.39
$^4D_{5/2}$	99559.33	1.37 ± 0.1	1.30	1.42
$^4H_{11/2}$	100309.29	1.30 ± 0.1	1.33	1.41
$^4G_{9/2}$	100619.26	1.25 ± 0.1	1.35	1.44

References. [(a)] Shenstone (1970); [(b)] Kurucz (2011).

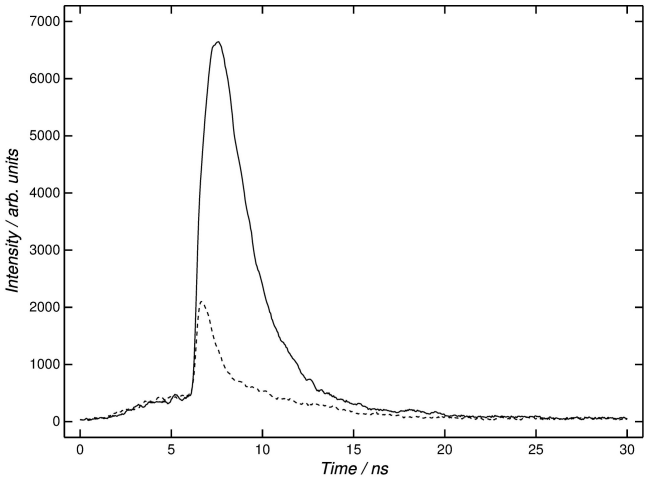

Fig. 2. First 30 ns of the decay of 4d $^4H_{13/2}$ in Ni II (solid line). Combined background contribution from both the first- and second-step lasers, where the latter is detuned 0.04 nm from resonance (dashed line). This background is substracted before the final lifetime analysis.

PM tube has a rise time of 200 ps and the oscilloscope sampled the decay and pulse shape at every 50 ps. All spectral measurements were performed in the second spectral order, which is closer to the optimum efficiency of the blazed grating, resulting in a linewidth of about 0.5 nm.

For both the first and the second excitations we used the frequency tripled output from Nd:YAG pumped dye lasers (Continuum Nd-60), primarily operating with DCM dye. The first step had a pulse length of 10 ns whereas, by injection seeding and compressing, for the second Nd:YAG laser a pulse length of about 1 ns could be obtained. Before every measurement the delay between the two lasers was checked and, if necessary, adjusted so that the short pulse from second laser coincided with the maximum population of the intermediate level. The short pulse length in the second step and the high time resolution of the detection system is necessary to accurately measure the short lifetimes involved (1.2−1.3 ns). To reach a sufficient statistical accuracy each decay curve was averaged over 1000 laser pulses. The final lifetime analysis used the code DECFIT (Palmeri et al. 2008) to fit a single exponential decay, convoluted by the measured pulse shape, and a background function to the observed decay curve. Typically 10 to 20 measurements, performed during different days, were averaged to obtain the final lifetimes, given in Table 2. The quoted uncertainties in the results are mainly due to the scatter between the individual measurements.

As discussed by Lundberg et al. (2016), two step measurements may lead to complicated blending situations that must be taken into account in the planning and execution of the experiment. In the Ni case, we note from Table 1 that the two excitation lasers as well as the fluorescence channels all occur in the narrow wavelength interval 210−226 nm. Thus, most of the recorded decay curves are influenced by the very intense decay from the intermediate levels. This contribution extends over more than 10ns, due to the length of the first step laser pulses, and is noticeable even at rather large wavelength differences. Fortunately, this effect may be accurately compensated for by subtracting a separate decay measurement, with the second step laser blocked, before the final lifetime analysis. A worse case is encountered in the measurement of the 4d $^4H_{13/2}$ level where also scattered light from the second laser influences the decay. This is illustrated in Fig. 2, and corrected for by a "background" measurement where the second laser is not blocked but detuned slightly from resonance. Finally, transitions from levels in the $3d^84p$ configuration populated through the decay of the 4d level under investigation, so called cascades, may cause blending problems. Since this cannot be compensated for, one has to carefully choose the fluorescence channels to use, and if no sufficiently intense channels remain this particular level has to be omitted from the investigation. An example of this is the failure to measure the 4d $^4G_{7/2}$ level at 100 475.8 cm^{-1} since all strong decay channels are blended by cascades.

3. Theoretical calculations

Calculations of energy levels and radiative transition rates in Ni II have been carried out using the relativistic Hartree-Fock (HFR) approach (Cowan 1981) modified to take core-polarization effects into account (Quinet et al. 1999, 2002). This method (HFR+CPOL) has been combined with a least-squares optimization process of the radial parameters to reduce the discrepancies between the Hamiltonian eigenvalues and the available experimental energy levels from Shenstone (1970). The following 23 configurations were explicitly introduced in the calculations: $3d^9$, $3d^84d$, $3d^85d$, $3d^74s4d$, $3d^74s5d$, $3d^64s^24d$, $3d^84s$, $3d^85s$, $3d^74s^2$, $3d^74s5s$, $3d^64s^25s$ for the even parity and $3d^84p$, $3d^85p$, $3d^74s4p$, $3d^74s5p$, $3d^64s^24p$, $3d^64s^25p$, $3d^84f$, $3d^85f$, $3d^74s4f$, $3d^74s5f$, $3d^64s^24f$, $3d^64s^25f$ for the odd parity.

The ionic core considered for the core-polarization model potential and the correction to the transition dipole operator was a $3d^6$ Ni V core. The dipole polarizability, α_d, for such a core is 0.94 a_0^3 according to Fraga et al. (1976). We used the HFR mean radius of the outermost 3d core orbital, 1.004 a_0, for the cut-off radius.

For the $3d^9$, $3d^84d$, $3d^85d$, $3d^84s$, $3d^85s$, $3d^74s^2$ even configurations and the $3d^84p$, $3d^85p$, $3d^74s4p$, $3d^84f$, $3d^85f$ odd configurations, the average energies (E_{av}), the electrostatic direct (F^k) and exchange (G^k) integrals, the spin-orbit (ζ_{nl}) and the effective interaction (α) parameters were allowed to vary during the fitting process. All other Slater integrals were scaled down by a factor 0.80 following a well-established procedure (Cowan 1981). The standard deviations of the fits were 212 cm^{-1} for the even parity and 77 cm^{-1} for the odd parity.

4. Results and discussion

The radiative lifetimes measured and computed in the present work are presented in Table 2. The theoretical lifetimes obtained in this work agree with the experimental values within about 5%.

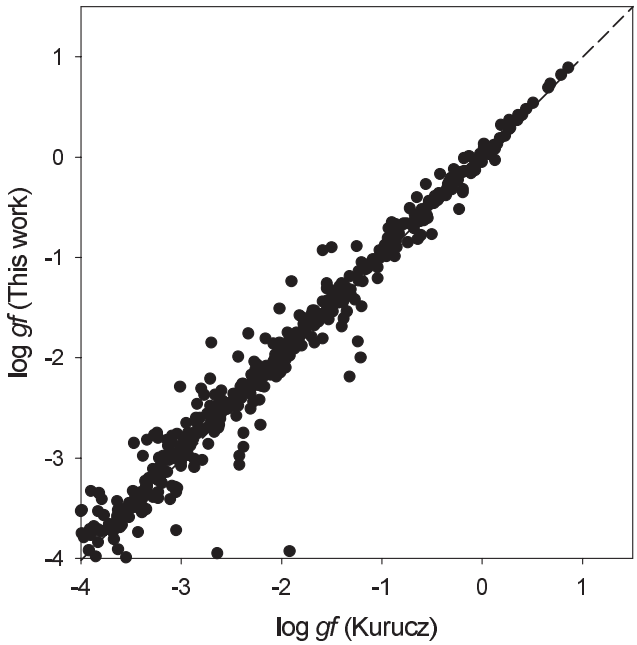

Fig. 3. Comparison between the oscillator strengths (log gf) calculated in the present work and those reported by Kurucz (2011) for transitions from highly excited even-parity $3d^84d$ levels in Ni II.

Table 2 includes the theoretical lifetimes obtained by Kurucz (2011). The latter work also used a semi-empirical approach based on a superposition of configurations calculation with a modified version of the Cowan codes (Cowan 1981) and experimental level energies (Shenstone 1970) to improve the results. In this case the calculated values are about 11% higher than the experiments.

Table A.1 presents the computed oscillator strengths and transition probabilities for the strongest transitions (log $gf > -4$) depopulating the even $3d^84d$ levels located in the range 98 467–103 664 cm^{-1}. This table also presents the cancellation factors (CF) as defined by Cowan (1981). Transitions with a CF lower than 0.05 should be considered with great care as they are affected by cancellation effects.

Most of the previous experimental and theoretical studies of radiative parameters in Ni II were focused on the spectral lines from the odd parity $3d^84p$ configuration ((Zsargó & Federman 1998; Fedchak & Lawler 1999; Fritzsche et al. 2000; Fedchak et al. 2000; Jenkins & Tripp 2006; Manrique et al. 2011) and the $3d^84s-3d^84p$ or $3d^9-3d^84p$ transitions. Recently, an extensive calculation of atomic structure data for Ni II was published by Cassidy et al. (2016). This work resulted in transition rates and oscillator strengths for 5023 electric dipole lines involving the $3d^9$, $3d^84s$, $3d^74s^2$, $3d^84p$ and $3d^74s4p$ configurations.

To our knowledge, the only work listing also oscillator strengths from the $3d^84d$ even levels is the database of Kurucz (2011). Figure 3 shows a good general agreement between the two data sets. However, a closer inspection reveals that our new oscillator strengths are systematically higher than the values by Kurucz (2011). The mean ratio gf(This work)/gf(Kurucz) is 1.22 for lines with log $gf > -4$. The new log gf values are thus on average 20% larger than the previous calculation by Kurucz (2011). The difference between the two sets of results is possibly due to different values of the radial dipole integrals in calculations of the line strengths. In the case of $3d^84p-3d^84d$ transition array for example, the reduced matrix element $\langle 4p||r^1||4d\rangle$ computed in our work was −4.55664 a.u. and −4.66532 a.u. with and without core-polarization, respectively, while, as far as we understand, Kurucz used a value scaled down to −4.47840 a.u. which tends to weaken the corresponding oscillator strengths.

5. Conclusion

We report seven new experimental radiative lifetimes for $3d^84d$ levels in Ni II, measured by two-step excitation using time-resolved laser-induced fluorescence on a laser ablation plasma. In addition, we report an extensive theoretical study using a relativistic Hartree-Fock technique optimized on experimental level energies. The theoretical and experimental lifetimes agree within 5%, which serves as benchmark for the accuracy of the 477 calculated oscillator strengths for the strong transitions around 200–220 nm belonging to the $3d^84p-3d^84d$ transition array. Furthermore, on a two-standard deviation level the new theoretical gf values as well as the results from Kurucz (2011) agree with the experimental lifetimes.

Acknowledgements. This work has received funding from LASERLAB-EUROPE (grant agreement No. 284464, EC's Seventh Framework Programme), the Swedish Research Council through the Linnaeus grant to the Lund Laser Centre and a VR project grant 621-2011-4206 (H.H.), and the Knut and Alice Wallenberg Foundation. P.P. and P.Q. are respectively Research Associate and Research Director of the Belgian National Fund for Scientific Research F.R.S.-FNRS from which financial support is gratefully acknowledged. V.F. acknowledges the Belgian Scientific Policy (BELSPO) for her Return Grant. P.Q., V.F., P.P., G.M. and K.B. are grateful to the colleagues from Lund Laser Center for their kind hospitality and support.

References

Brandt, J. C., Heap, S. R., Beaver, E. A., et al. 1999, AJ, 117, 1505
Cassidy, C. M., Hibbert, A., & Ramsbottom, C. A. 2016, A&A, 587, A107
Cowan, R. D. 1981, The theory of atomic structure and spectra (Berkeley: University of California Press)
Engström, L., Lundberg, H., Nilsson, H., Hartman, H., & Bäckström, E. 2014, A&A, 570, A34
Fedchak, J. A., & Lawler, J. E. 1999, ApJ, 523, 734
Fedchak, J. A., Wiese, L. M., & Lawler, J. E. 2000, ApJ, 538, 773
Fraga, S., Karwowski, J., & Saxena, K. 1976, Handbook of Atomic Data (Amsterdam: Elsevier)
Fritzsche, S., Dong, C. Z., & Gaigalas, G. 2000, Atom. Data Nucl. Data Tables, 76, 155
Hartman, H., Nilsson, H., Engström, L., & Lundberg, H. 2015, A&A, 584, A24
Hinkle, K., Wallace, L., Valenti, J., & Ayres, T. 2005, Ultraviolet Atlas of the Arcturus Spectrum, 1150–3800 Å. (San Francisco: ASP)
Jenkins, E. B., & Tripp, T. M. 2006, ApJ, 637, 548
Kurucz, R. 2011, http://kurucz.harvard.edu
Lawler, J. E., & Salih, S. 1987, Phys. Rev. A, 35, 5046
Lind, K., Bergemann, M., & Asplund, M. 2012, MNRAS, 427, 50
Lundberg, H., Hartman, H., Engström, L., et al. 2016, MNRAS, 460, 356
Manrique, J., Aguilera, J. A., & Aragón, C. 2011, J. Quant. Spectr. Rad. Transf., 112, 85
Moore, C. E. 1959, A multiplet table of astrophysical interest, Part 1 (NBS Technical Note, Washington: US Department of Commerce)
Nadyozhin, D. K. 2003, MNRAS, 346, 97
Palmeri, P., Quinet, P., Fivet, V., et al. 2008, Phys. Scr., 78, 015304
Quinet, P., Palmeri, P., Biémont, E., et al. 1999, MNRAS, 307, 934
Quinet, P., Palmeri, P., Biémont, E., et al. 2002, J. Alloys Comp., 344, 255
Quinet, P., Fivet, V., Palmeri, P., et al. 2016, MNRAS, 462, 3912
Shenstone, A. 1970, J. Res. Natl. Bur. Stand., 76A, 801
Stritzinger, M., Mazzali, P. A., Sollerman, J., & Benetti, S. 2006, A&A, 460, 793
Wongwathanarat, A., Janka, H.-T., & Müller, E. 2011, in Death of Massive Stars: Supernovae and Gamma-Ray Bursts, Proc. IAU Symp., 7, 150
Zsargó, J., & Federman, S. R. 1998, ApJ, 498, 256

Appendix A: Additional table

Table A.1. Transition probabilities and oscillator strengths for spectral lines depopulating highly excited levels belonging to the even-parity $3d^8 4d$ configuration of Ni II.

λ^a (nm)	Lower odd level^b		Upper 4d level^b		HFR+CPOL^c		
	E (cm^{-1})	J	E (cm^{-1})	J	log gf	gA (s^{-1})	CF
194.2965	51 558	3.5	103 026	2.5	−2.69	3.64E+06	0.018
196.3670	52 738	2.5	103 664	1.5	−3.74	3.12E+05	0.003
198.8580	52 738	2.5	103 026	2.5	−1.82	2.58E+07	0.077
199.2730	51 558	3.5	101 740	3.5	−3.04	1.54E+06	0.004
199.8845	53 635	1.5	103 664	1.5	−2.23	9.76E+06	0.100
200.7049	51 558	3.5	101 366	2.5	−3.20	1.04E+06	0.003
200.7409	51 558	3.5	101 357	4.5	−2.21	1.02E+07	0.054
201.1847	51 558	3.5	101 247	2.5	−3.36	7.19E+05	0.015
201.6016	51 558	3.5	101 145	3.5	−2.86	2.25E+06	0.009
202.0071	54 176	0.5	103 664	1.5	−2.96	1.80E+06	0.057
202.4010	53 635	1.5	103 026	2.5	−1.97	1.75E+07	0.237
203.7607	51 558	3.5	100 619	4.5	−0.93	1.90E+08	0.160
203.8699	51 558	3.5	100 593	3.5	−2.67	3.44E+06	0.002
204.0085	52 738	2.5	101 740	3.5	−1.19	1.03E+08	0.166
204.3583	51 558	3.5	100 476	3.5	−2.36	7.01E+06	0.020
204.7195	51 558	3.5	100 390	2.5	−1.91	1.96E+07	0.022
204.9606	51 558	3.5	100 332	4.5	−3.71	3.10E+05	0.004
205.5061	55 019	2.5	103 664	1.5	−2.47	5.32E+06	0.222
205.5783	52 738	2.5	101 366	2.5	−1.57	4.25E+07	0.031
206.0365	52 738	2.5	101 258	1.5	−2.17	1.06E+07	0.016
206.0817	52 738	2.5	101 247	2.5	−1.82	2.40E+07	0.082
206.5192	52 738	2.5	101 145	3.5	−1.53	4.61E+07	0.090
206.6519	53 365	4.5	101 740	3.5	−3.00	1.54E+06	0.003
208.2372	55 019	2.5	103 026	2.5	−3.28	8.07E+05	0.021
208.2606	51 558	3.5	99 559	2.5	−0.93	1.79E+08	0.041
208.3016	53 365	4.5	101 357	4.5	−3.84	2.20E+05	0.000
208.7672	51 558	3.5	99 443	4.5	−0.40	6.10E+08	0.347
208.9002	52 738	2.5	100 593	3.5	−0.25	8.54E+08	0.424
209.2143	51 558	3.5	99 341	3.5	−1.07	1.31E+08	0.252
209.2284	53 365	4.5	101 145	3.5	−3.53	4.45E+05	0.001
209.3466	52 738	2.5	100 491	1.5	−0.58	3.99E+08	0.116
209.4129	52 738	2.5	100 476	3.5	−0.90	1.89E+08	0.453
209.4386	53 635	1.5	101 366	2.5	−0.44	5.46E+08	0.354
209.7923	52 738	2.5	100 390	2.5	−2.29	7.72E+06	0.004
209.9142	53 635	1.5	101 258	1.5	−1.40	6.04E+07	0.045
209.9611	53 635	1.5	101 247	2.5	−1.02	1.43E+08	0.460
209.9665	53 635	1.5	101 246	0.5	−0.65	3.38E+08	0.605
209.9832	55 418	3.5	103 026	2.5	−1.45	5.42E+07	0.098
210.0308	51 558	3.5	99 155	4.5	−0.05	1.35E+09	0.675
210.0693	56 075	2.5	103 664	1.5	−2.28	7.95E+06	0.036
210.5587	54 263	3.5	101 740	3.5	−2.98	1.56E+06	0.001
211.1695	52 738	2.5	100 079	1.5	−0.17	1.01E+09	0.619
211.5549	53 365	4.5	100 619	4.5	−1.97	1.59E+07	0.004
211.6225	56 424	1.5	103 664	1.5	−1.52	4.55E+07	0.287
211.6727	53 365	4.5	100 593	3.5	−1.53	4.44E+07	0.045
211.7490	53 635	1.5	100 845	0.5	−1.84	2.17E+07	0.015
211.8727	54 557	4.5	101 740	3.5	−3.53	4.39E+05	0.001
212.1445	53 496	5.5	100 619	4.5	−2.80	2.33E+06	0.005
212.1991	53 365	4.5	100 476	3.5	−1.91	1.83E+07	0.030
212.2313	54 263	3.5	101 366	2.5	−1.60	3.74E+07	0.029
212.2716	54 263	3.5	101 357	4.5	−2.67	3.14E+06	0.001
212.3294	54 176	0.5	101 258	1.5	−0.14	1.06E+09	0.836
212.3829	54 176	0.5	101 246	0.5	−0.93	1.72E+08	0.381

Notes. xE+y stands for $x \times 10^y$. Only transitions with log $gf \geq -4.0$ are listed in the table. [a] Vacuum ($\lambda < 200$ nm) and air ($\lambda > 200$ nm) Ritz wavelengths deduced from the experimental energy level values by Shenstone (1970); [b] Energies from Shenstone (1970). Energy values have been rounded to the nearest unit; [c] This work.

Table A.1. continued.

λ^a (nm)	Lower odd level^b		Upper 4d level^b		HFR+CPOL^c		
	E (cm^{-1})	J	E (cm^{-1})	J	log gf	gA (s^{-1})	CF
212.6835	51 558	3.5	98 561	2.5	0.48	4.47E+09	0.859
212.7678	54 263	3.5	101 247	2.5	−1.36	6.45E+07	0.108
212.8486	53 365	4.5	100 332	4.5	−1.71	2.83E+07	0.013
212.9239	56 075	2.5	103 026	2.5	−1.90	1.85E+07	0.073
212.9520	53 365	4.5	100 309	5.5	−1.21	9.12E+07	0.009
213.1096	51 558	3.5	98 467	3.5	0.41	3.78E+09	0.736
213.2342	54 263	3.5	101 145	3.5	−1.29	7.50E+07	0.024
213.3510	53 635	1.5	100 491	1.5	0.09	1.82E+09	0.775
213.5126	52 738	2.5	99 559	2.5	0.30	2.90E+09	0.744
213.5494	53 496	5.5	100 309	5.5	−1.86	2.02E+07	0.013
213.8139	53 635	1.5	100 390	2.5	−0.23	8.53E+08	0.708
213.9665	55 019	2.5	101 740	3.5	−1.12	1.10E+08	0.182
214.2068	54 176	0.5	100 845	0.5	−0.14	1.07E+09	0.852
214.2756	56 371	3.5	103 026	2.5	−1.64	3.34E+07	0.075
214.5150	52 738	2.5	99 341	3.5	−0.38	6.08E+08	0.617
214.5197	56 424	1.5	103 026	2.5	−2.15	1.02E+07	0.211
214.5819	54 557	4.5	101 145	3.5	−2.94	1.67E+06	0.011
215.2446	53 635	1.5	100 079	1.5	−0.78	2.40E+08	0.187
215.2610	55 300	4.5	101 740	3.5	−3.29	7.29E+05	0.001
215.5631	53 635	1.5	100 010	0.5	−0.14	1.04E+09	0.866
215.6511	54 263	3.5	100 619	4.5	−0.99	1.46E+08	0.038
215.6939	55 019	2.5	101 366	2.5	−0.61	3.51E+08	0.149
215.7734	54 263	3.5	100 593	3.5	−2.00	1.44E+07	0.007
215.8103	55 418	3.5	101 740	3.5	−1.81	2.21E+07	0.009
215.8464	54 176	0.5	100 491	1.5	−0.88	1.89E+08	0.238
215.9041	52 738	2.5	99 041	1.5	0.03	1.54E+09	0.868
216.1795	57 420	2.5	103 664	1.5	−0.49	4.60E+08	0.318
216.1983	55 019	2.5	101 258	1.5	−0.63	3.32E+08	0.435
216.2481	55 019	2.5	101 247	2.5	−0.18	9.38E+08	0.674
216.3205	54 263	3.5	100 476	3.5	0.10	1.78E+09	0.619
216.7253	54 263	3.5	100 390	2.5	−0.64	3.26E+08	0.291
216.7298	55 019	2.5	101 145	3.5	0.21	2.26E+09	0.369
216.9567	53 365	4.5	99 443	4.5	−0.52	4.32E+08	0.139
216.9955	54 263	3.5	100 332	4.5	0.41	3.60E+09	0.495
217.0296	54 557	4.5	100 619	4.5	−3.95	1.58E+05	0.000
217.0516	55 300	4.5	101 357	4.5	−1.45	5.07E+07	0.030
217.1535	54 557	4.5	100 593	3.5	−1.57	3.83E+07	0.043
217.4396	53 365	4.5	99 341	3.5	−0.32	6.76E+08	0.732
217.5677	55 418	3.5	101 366	2.5	−2.36	6.21E+06	0.005
217.5769	53 496	5.5	99 443	4.5	−0.89	1.81E+08	0.397
217.5832	57 081	3.5	103 026	2.5	−0.15	9.98E+08	0.540
217.6100	55 418	3.5	101 357	4.5	−0.87	1.92E+08	0.055
217.6795	53 635	1.5	99 559	2.5	−1.07	1.20E+08	0.076
217.7077	54 557	4.5	100 476	3.5	−2.10	1.13E+07	0.035
217.7847	54 176	0.5	100 079	1.5	−1.37	5.97E+07	0.095
218.1108	54 176	0.5	100 010	0.5	−1.54	4.02E+07	0.042
218.1316	55 418	3.5	101 247	2.5	−2.39	5.70E+06	0.010
218.1638	52 738	2.5	98 561	2.5	−1.62	3.36E+07	0.011
218.3217	53 365	4.5	99 155	4.5	0.37	3.25E+09	0.754
218.3913	54 557	4.5	100 332	4.5	−1.76	2.43E+07	0.045
218.4268	53 365	4.5	99 133	5.5	−0.35	6.22E+08	0.117
218.5002	54 557	4.5	100 309	5.5	−3.01	1.36E+06	0.000
218.6122	52 738	2.5	98 467	3.5	−1.02	1.34E+08	0.090
218.6217	55 418	3.5	101 145	3.5	−1.26	7.63E+07	0.035
218.9176	56 075	2.5	101 740	3.5	−0.69	2.83E+08	0.136
218.9497	53 496	5.5	99 155	4.5	−0.32	6.61E+08	0.876
219.0554	53 496	5.5	99 133	5.5	0.13	1.86E+09	0.732
219.2037	57 420	2.5	103 026	2.5	−0.21	8.65E+08	0.205

Table A.1. continued.

λ^a (nm)	Lower odd level^b		Upper 4d level^b		HFR+CPOL^c		
	E (cm^{-1})	J	E (cm^{-1})	J	log gf	gA (s^{-1})	CF
219.2092	53 365	4.5	98 969	5.5	0.73	7.40E+09	0.765
219.3535	55 019	2.5	100 593	3.5	−0.01	1.35E+09	0.770
219.8423	53 496	5.5	98 969	5.5	0.13	1.87E+09	0.918
219.8457	55 019	2.5	100 491	1.5	−1.05	1.23E+08	0.574
219.9189	55 019	2.5	100 476	3.5	0.01	1.40E+09	0.397
220.1659	53 635	1.5	99 041	1.5	−3.92	1.66E+05	0.000
220.3373	55 019	2.5	100 390	2.5	−0.24	7.93E+08	0.559
220.3467	56 371	3.5	101 740	3.5	0.06	1.58E+09	0.551
220.5548	53 496	5.5	98 823	6.5	0.89	1.06E+10	0.928
220.5862	55 300	4.5	100 619	4.5	0.28	2.62E+09	0.710
220.6978	54 263	3.5	99 559	2.5	−0.36	6.06E+08	0.702
220.7142	55 300	4.5	100 593	3.5	−0.81	2.12E+08	0.283
220.7262	56 075	2.5	101 366	2.5	−0.21	8.43E+08	0.224
221.1630	55 418	3.5	100 619	4.5	−0.01	1.33E+09	0.245
221.2544	56 075	2.5	101 258	1.5	−2.19	8.86E+06	0.008
221.2668	54 263	3.5	99 443	4.5	0.08	1.65E+09	0.636
221.2867	55 300	4.5	100 476	3.5	−0.64	3.12E+08	0.587
221.2917	55 418	3.5	100 593	3.5	0.03	1.45E+09	0.423
221.3066	56 075	2.5	101 247	2.5	−1.32	6.60E+07	0.035
221.3155	58 493	2.5	103 664	1.5	−0.41	5.31E+08	0.319
221.6502	53 365	4.5	98 467	3.5	−0.46	4.68E+08	0.732
221.7690	54 263	3.5	99 341	3.5	−0.04	1.25E+09	0.589
221.8111	56 075	2.5	101 145	3.5	0.42	3.57E+09	0.943
221.8569	55 019	2.5	100 079	1.5	−1.11	1.04E+08	0.456
221.8671	55 418	3.5	100 476	3.5	−1.51	4.19E+07	0.016
221.9930	55 300	4.5	100 332	4.5	−0.71	2.66E+08	0.141
222.1055	55 300	4.5	100 309	5.5	0.82	8.89E+09	0.955
222.1791	56 371	3.5	101 366	2.5	−1.30	6.83E+07	0.257
222.2233	56 371	3.5	101 357	4.5	0.54	4.62E+09	0.640
222.2929	55 418	3.5	100 390	2.5	−1.58	3.61E+07	0.026
222.3629	58 706	1.5	103 664	1.5	0.09	1.67E+09	0.679
222.4415	56 424	1.5	101 366	2.5	0.19	2.11E+09	0.859
222.5161	53 635	1.5	98 561	2.5	−1.94	1.57E+07	0.017
222.5772	55 418	3.5	100 332	4.5	0.42	3.50E+09	0.950
222.6867	54 263	3.5	99 155	4.5	−0.27	7.25E+08	0.183
222.7183	54 557	4.5	99 443	4.5	0.32	2.84E+09	0.769
222.7672	56 371	3.5	101 247	2.5	−0.43	4.97E+08	0.858
222.8241	54 176	0.5	99 041	1.5	−2.29	6.93E+06	0.018
222.9781	56 424	1.5	101 258	1.5	0.06	1.56E+09	0.779
223.0310	56 424	1.5	101 247	2.5	−0.27	7.28E+08	0.429
223.0370	56 424	1.5	101 246	0.5	−1.69	2.75E+07	0.297
223.2272	54 557	4.5	99 341	3.5	−1.87	1.81E+07	0.033
223.2784	56 371	3.5	101 145	3.5	−1.31	6.48E+07	0.073
223.8459	57 081	3.5	101 740	3.5	−0.43	4.96E+08	0.235
224.1569	54 557	4.5	99 155	4.5	−0.03	1.25E+09	0.348
224.2677	54 557	4.5	99 133	5.5	0.69	6.47E+09	0.972
224.4445	55 019	2.5	99 559	2.5	−3.35	5.98E+05	0.001
224.4861	58 493	2.5	103 026	2.5	0.09	1.63E+09	0.685
224.5600	56 075	2.5	100 593	3.5	−0.77	2.23E+08	0.135
225.0494	56 424	1.5	100 845	0.5	−0.73	2.47E+08	0.672
225.0759	56 075	2.5	100 491	1.5	−0.68	2.74E+08	0.408
225.0926	54 557	4.5	98 969	5.5	−2.19	8.53E+06	0.002
225.1526	56 075	2.5	100 476	3.5	−0.36	5.72E+08	0.171
225.5525	55 019	2.5	99 341	3.5	−1.81	2.05E+07	0.028
225.5613	57 420	2.5	101 740	3.5	−0.71	2.54E+08	0.179
225.5638	58 706	1.5	103 026	2.5	−0.46	4.59E+08	0.695
225.5911	56 075	2.5	100 390	2.5	−0.06	1.14E+09	0.414
225.6709	54 263	3.5	98 561	2.5	−1.35	5.87E+07	0.151

Table A.1. continued.

λ^a (nm)	Lower odd level^b		Upper 4d level^b		HFR+CPOL^c		
	E (cm^{-1})	J	E (cm^{-1})	J	log gf	gA (s^{-1})	CF
225.7372	57 081	3.5	101 366	2.5	−1.68	2.74E+07	0.073
225.7828	57 081	3.5	101 357	4.5	0.29	2.54E+09	0.970
225.9297	56 371	3.5	100 619	4.5	0.12	1.71E+09	0.545
226.0640	56 371	3.5	100 593	3.5	−0.52	3.92E+08	0.350
226.1507	54 263	3.5	98 467	3.5	−1.75	2.33E+07	0.040
226.3443	57 081	3.5	101 247	2.5	−1.10	1.03E+08	0.168
226.4653	55 300	4.5	99 443	4.5	−3.52	3.97E+05	0.000
226.4741	55 418	3.5	99 559	2.5	−0.27	7.12E+08	0.428
226.6646	56 371	3.5	100 476	3.5	−0.63	3.06E+08	0.274
226.8598	56 424	1.5	100 491	1.5	−2.82	1.97E+06	0.004
226.8721	57 081	3.5	101 145	3.5	−2.40	5.11E+06	0.008
226.9915	55 300	4.5	99 341	3.5	−1.97	1.40E+07	0.017
227.0733	55 418	3.5	99 443	4.5	−0.32	6.27E+08	0.215
227.0887	55 019	2.5	99 041	1.5	−2.15	9.02E+06	0.079
227.1090	56 371	3.5	100 390	2.5	−1.29	6.68E+07	0.141
227.1843	56 075	2.5	100 079	1.5	−0.61	3.17E+08	0.373
227.3832	56 424	1.5	100 390	2.5	−1.43	4.84E+07	0.031
227.4057	56 371	3.5	100 332	4.5	−3.93	1.52E+05	0.000
227.4818	57 420	2.5	101 366	2.5	−0.90	1.60E+08	0.541
227.6023	55 418	3.5	99 341	3.5	−0.03	1.20E+09	0.364
227.6672	54 557	4.5	98 467	3.5	0.09	1.59E+09	0.901
227.9529	55 300	4.5	99 155	4.5	−1.81	2.00E+07	0.006
228.0430	57 420	2.5	101 258	1.5	−3.58	3.37E+05	0.021
228.0675	55 300	4.5	99 133	5.5	−1.61	3.17E+07	0.007
228.0983	57 420	2.5	101 247	2.5	−0.12	9.78E+08	0.702
228.5689	55 418	3.5	99 155	4.5	−0.51	4.01E+08	0.079
228.6343	57 420	2.5	101 145	3.5	−2.21	7.89E+06	0.036
228.9207	55 300	4.5	98 969	5.5	−1.49	4.15E+07	0.005
229.0019	56 424	1.5	100 079	1.5	−1.66	2.80E+07	0.059
229.3625	56 424	1.5	100 010	0.5	−0.99	1.31E+08	0.255
229.5899	55 019	2.5	98 561	2.5	−2.71	2.50E+06	0.019
229.6099	57 081	3.5	100 619	4.5	0.04	1.37E+09	0.373
229.7486	57 081	3.5	100 593	3.5	−0.20	7.98E+08	0.486
230.0865	55 019	2.5	98 467	3.5	−3.33	5.96E+05	0.008
230.3689	57 081	3.5	100 476	3.5	−0.13	9.27E+08	0.437
230.8280	57 081	3.5	100 390	2.5	−1.29	6.46E+07	0.116
231.0611	56 075	2.5	99 341	3.5	−1.66	2.73E+07	0.015
231.1346	57 081	3.5	100 332	4.5	−0.69	2.56E+08	0.100
231.1585	58 493	2.5	101 740	3.5	0.37	2.88E+09	0.937
231.5560	57 420	2.5	100 593	3.5	−0.41	4.80E+08	0.666
231.5840	55 300	4.5	98 467	3.5	−1.37	5.36E+07	0.130
231.7140	55 418	3.5	98 561	2.5	−1.01	1.22E+08	0.136
231.7599	56 424	1.5	99 559	2.5	−2.56	3.43E+06	0.009
232.1011	56 371	3.5	99 443	4.5	−0.65	2.79E+08	0.136
232.1046	57 420	2.5	100 491	1.5	−0.82	1.86E+08	0.575
232.1862	57 420	2.5	100 476	3.5	−0.85	1.74E+08	0.211
232.2198	55 418	3.5	98 467	3.5	−1.40	4.92E+07	0.037
232.6525	57 420	2.5	100 390	2.5	−0.39	5.00E+08	0.647
232.6537	56 371	3.5	99 341	3.5	−0.76	2.13E+08	0.156
232.6735	56 075	2.5	99 041	1.5	−1.54	3.57E+07	0.073
233.1759	58 493	2.5	101 366	2.5	−0.96	1.34E+08	0.207
233.6639	56 371	3.5	99 155	4.5	−1.76	2.13E+07	0.022
233.7655	58 493	2.5	101 258	1.5	−3.41	4.75E+05	0.008
233.8237	58 493	2.5	101 247	2.5	−0.35	5.39E+08	0.250
234.3388	58 706	1.5	101 366	2.5	−0.84	1.75E+08	0.533
234.3474	57 420	2.5	100 079	1.5	−0.11	9.41E+08	0.948
234.3870	58 493	2.5	101 145	3.5	−1.85	1.69E+07	0.026
234.5804	56 424	1.5	99 041	1.5	−2.44	4.44E+06	0.019

Table A.1. continued.

λ^a (nm)	Lower odd level^b		Upper 4d level^b		HFR+CPOL^c		
	E (cm^{-1})	J	E (cm^{-1})	J	log gf	gA (s^{-1})	CF
234.9343	58 706	1.5	101 258	1.5	−1.58	3.16E+07	0.335
234.9931	58 706	1.5	101 247	2.5	−0.64	2.73E+08	0.259
234.9998	58 706	1.5	101 246	0.5	−0.16	8.32E+08	0.917
235.2999	56 075	2.5	98 561	2.5	−2.04	1.11E+07	0.022
235.3396	57 081	3.5	99 559	2.5	−2.27	6.45E+06	0.015
235.8215	56 075	2.5	98 467	3.5	−2.74	2.19E+06	0.008
235.9867	57 081	3.5	99 443	4.5	−0.18	7.82E+08	0.259
236.5581	57 081	3.5	99 341	3.5	−0.15	8.49E+08	0.251
236.9517	56 371	3.5	98 561	2.5	−2.31	5.79E+06	0.461
237.2348	58 706	1.5	100 845	0.5	−0.90	1.49E+08	0.420
237.2365	57 420	2.5	99 559	2.5	−1.38	4.95E+07	0.130
237.2502	56 424	1.5	98 561	2.5	−3.15	8.43E+05	0.010
237.4585	58 493	2.5	100 593	3.5	−1.14	8.48E+07	0.073
237.4807	56 371	3.5	98 467	3.5	−2.16	8.18E+06	0.168
237.6025	57 081	3.5	99 155	4.5	−1.24	6.81E+07	0.037
238.0354	58 493	2.5	100 491	1.5	−1.42	4.45E+07	0.214
238.1212	58 493	2.5	100 476	3.5	−0.66	2.55E+08	0.256
238.4747	57 420	2.5	99 341	3.5	−0.26	6.41E+08	0.430
238.6117	58 493	2.5	100 390	2.5	−0.80	1.85E+08	0.118
239.2474	58 706	1.5	100 491	1.5	−2.89	1.51E+06	0.008
239.8296	58 706	1.5	100 390	2.5	−0.57	3.08E+08	0.426
240.1926	57 420	2.5	99 041	1.5	−0.12	8.73E+08	0.653
240.3949	58 493	2.5	100 079	1.5	−0.95	1.29E+08	0.288
241.0028	57 081	3.5	98 561	2.5	−1.63	2.70E+07	0.268
241.5501	57 081	3.5	98 467	3.5	−1.63	2.68E+07	0.100
241.6311	58 706	1.5	100 079	1.5	−1.23	6.68E+07	0.297
242.0325	58 706	1.5	100 010	0.5	−0.67	2.44E+08	0.626
242.9924	57 420	2.5	98 561	2.5	−3.12	8.66E+05	0.021
243.4359	58 493	2.5	99 559	2.5	−3.33	5.33E+05	0.001
243.5488	57 420	2.5	98 467	3.5	−2.29	5.78E+06	0.097
244.7036	58 706	1.5	99 559	2.5	−2.07	9.57E+06	0.071
244.7398	58 493	2.5	99 341	3.5	−1.07	9.53E+07	0.063
246.5495	58 493	2.5	99 041	1.5	−0.66	2.42E+08	0.418
247.8500	58 706	1.5	99 041	1.5	−1.33	5.07E+07	0.147
250.0870	58 493	2.5	98 467	3.5	−2.75	1.91E+06	0.036
269.5188	66 571	2.5	103 664	1.5	−3.65	2.05E+05	0.005
269.5796	66 580	1.5	103 664	1.5	−2.51	2.83E+06	0.025
272.9010	67 031	0.5	103 664	1.5	−2.86	1.25E+06	0.077
274.2354	66 571	2.5	103 026	2.5	−2.27	4.75E+06	0.040
274.2984	66 580	1.5	103 026	2.5	−2.13	6.59E+06	0.120
277.9362	67 695	2.5	103 664	1.5	−2.19	5.63E+06	0.080
281.5343	68 154	1.5	103 664	1.5	−1.64	1.91E+07	0.060
282.5474	68 282	0.5	103 664	1.5	−2.28	4.42E+06	0.081
282.9548	67 695	2.5	103 026	2.5	−2.48	2.76E+06	0.055
286.2231	68 736	2.5	103 664	1.5	−3.57	2.19E+05	0.003
286.4951	68 131	3.5	103 026	2.5	−1.94	9.48E+06	0.227
286.6848	68 154	1.5	103 026	2.5	−2.04	7.41E+06	0.081
287.3149	66 571	2.5	101 366	2.5	−3.36	3.55E+05	0.013
288.1178	68 966	1.5	103 664	1.5	−1.90	1.01E+07	0.096
288.2991	66 571	2.5	101 247	2.5	−2.44	2.93E+06	0.074
288.3687	66 580	1.5	101 247	2.5	−2.60	2.00E+06	0.056
288.3788	66 580	1.5	101 246	0.5	−2.10	6.30E+06	0.250
289.1558	66 571	2.5	101 145	3.5	−3.68	1.66E+05	0.012
291.5482	68 736	2.5	103 026	2.5	−2.28	4.08E+06	0.020
291.7516	66 580	1.5	100 845	0.5	−2.37	3.32E+06	0.213
292.0816	67 031	0.5	101 258	1.5	−3.25	4.43E+05	0.145
292.1827	67 031	0.5	101 246	0.5	−3.77	1.31E+05	0.070
293.5143	68 966	1.5	103 026	2.5	−2.26	4.27E+06	0.062
293.6376	67 695	2.5	101 740	3.5	−2.04	7.09E+06	0.183

Table A.1. continued.

λ^a (nm)	Lower odd level^b		Upper 4d level^b		HFR+CPOL^c		
	E (cm^{-1})	J	E (cm^{-1})	J	log gf	gA (s^{-1})	CF
293.8446	66 571	2.5	100 593	3.5	−4.00	7.73E+04	0.003
294.8601	66 571	2.5	100 476	3.5	−2.51	2.34E+06	0.107
295.6126	66 571	2.5	100 390	2.5	−2.82	1.15E+06	0.049
295.6457	67 031	0.5	100 845	0.5	−3.92	9.29E+04	0.022
295.6857	66 580	1.5	100 390	2.5	−2.08	6.30E+06	0.330
296.9004	67 695	2.5	101 366	2.5	−2.82	1.16E+06	0.038
297.4520	68 131	3.5	101 740	3.5	−3.69	1.52E+05	0.004
297.9514	67 695	2.5	101 247	2.5	−2.12	5.68E+06	0.128
298.3541	66 571	2.5	100 079	1.5	−1.98	7.77E+06	0.297
298.7778	67 031	0.5	100 491	1.5	−3.04	6.86E+05	0.156
298.8666	67 695	2.5	101 145	3.5	−3.25	4.17E+05	0.006
299.0412	66 580	1.5	100 010	0.5	−2.48	2.46E+06	0.213
300.8815	68 131	3.5	101 357	4.5	−3.10	5.90E+05	0.007
301.0098	68 154	1.5	101 366	2.5	−2.66	1.61E+06	0.035
302.0902	68 154	1.5	101 247	2.5	−1.72	1.39E+07	0.148
302.1012	68 154	1.5	101 246	0.5	−1.44	2.63E+07	0.534
302.5043	67 031	0.5	100 079	1.5	−3.19	4.67E+05	0.191
302.6849	70 635	2.5	103 664	1.5	−3.16	5.07E+05	0.042
302.9027	68 736	2.5	101 740	3.5	−2.19	4.67E+06	0.096
303.0524	66 571	2.5	99 559	2.5	−2.74	1.34E+06	0.037
303.1293	66 580	1.5	99 559	2.5	−2.70	1.47E+06	0.093
303.1336	67 031	0.5	100 010	0.5	−3.14	5.32E+05	0.187
303.3399	70 707	1.5	103 664	1.5	−3.22	4.44E+05	0.038
303.8783	67 695	2.5	100 593	3.5	−2.76	1.27E+06	0.033
304.8237	67 695	2.5	100 491	1.5	−3.68	1.50E+05	0.016
305.0758	66 571	2.5	99 341	3.5	−1.87	9.75E+06	0.338
305.7694	67 695	2.5	100 390	2.5	−2.60	1.80E+06	0.077
305.8047	68 154	1.5	100 845	0.5	−1.99	7.23E+06	0.268
306.3759	68 736	2.5	101 366	2.5	−3.27	3.79E+05	0.010
307.0003	68 282	0.5	100 845	0.5	−3.54	2.04E+05	0.024
307.4952	68 736	2.5	101 247	2.5	−2.67	1.50E+06	0.026
307.7161	68 131	3.5	100 619	4.5	−2.26	3.91E+06	0.132
307.8927	66 571	2.5	99 041	1.5	−1.66	1.54E+07	0.486
307.9652	68 131	3.5	100 593	3.5	−2.60	1.75E+06	0.078
307.9721	66 580	1.5	99 041	1.5	−2.65	1.56E+06	0.120
308.4700	68 736	2.5	101 145	3.5	−3.41	2.68E+05	0.014
308.5477	68 966	1.5	101 366	2.5	−3.45	2.50E+05	0.009
308.7035	67 695	2.5	100 079	1.5	−3.91	8.49E+04	0.012
309.0808	68 131	3.5	100 476	3.5	−2.48	2.29E+06	0.165
309.1570	68 154	1.5	100 491	1.5	−3.82	1.06E+05	0.006
309.6829	68 966	1.5	101 247	2.5	−2.29	3.59E+06	0.119
309.6946	68 966	1.5	101 246	0.5	−2.35	3.07E+06	0.202
309.9077	68 131	3.5	100 390	2.5	−3.71	1.35E+05	0.015
310.0120	70 778	3.5	103 026	2.5	−2.73	1.30E+06	0.089
310.1298	68 154	1.5	100 390	2.5	−1.88	9.15E+06	0.207
310.4604	68 131	3.5	100 332	4.5	−2.85	9.72E+05	0.037
312.3145	67 031	0.5	99 041	1.5	−3.29	3.48E+05	0.161
312.5083	66 571	2.5	98 561	2.5	−3.40	2.75E+05	0.020
312.5900	66 580	1.5	98 561	2.5	−2.92	8.34E+05	0.183
313.1486	68 154	1.5	100 079	1.5	−2.16	4.69E+06	0.273
313.4290	66 571	2.5	98 467	3.5	−2.02	6.46E+06	0.433
313.4608	71 771	2.5	103 664	1.5	−2.58	1.77E+06	0.171
313.5878	68 966	1.5	100 845	0.5	−2.75	1.21E+06	0.080
313.7361	67 695	2.5	99 559	2.5	−2.29	3.50E+06	0.249
313.8118	68 736	2.5	100 593	3.5	−2.45	2.38E+06	0.129
313.8231	68 154	1.5	100 010	0.5	−1.85	9.65E+06	0.415
314.4024	68 282	0.5	100 079	1.5	−3.52	2.05E+05	0.065
314.8202	68 736	2.5	100 491	1.5	−2.42	2.53E+06	0.148

Table A.1. continued.

λ^a (nm)	Lower odd level^b		Upper 4d level^b		HFR+CPOL^c		
	E (cm^{-1})	J	E (cm^{-1})	J	log gf	gA (s^{-1})	CF
314.9702	68 736	2.5	100 476	3.5	−1.80	1.06E+07	0.355
315.0823	68 282	0.5	100 010	0.5	−3.66	1.48E+05	0.035
315.8290	68 736	2.5	100 390	2.5	−3.52	1.99E+05	0.011
315.9051	67 695	2.5	99 341	3.5	−2.79	1.08E+06	0.060
318.0944	68 131	3.5	99 559	2.5	−2.48	2.22E+06	0.099
318.1374	68 966	1.5	100 390	2.5	−2.43	2.47E+06	0.220
318.3284	68 154	1.5	99 559	2.5	−2.88	8.74E+05	0.055
318.9266	67 695	2.5	99 041	1.5	−2.35	2.93E+06	0.290
318.9603	68 736	2.5	100 079	1.5	−1.54	1.85E+07	0.617
319.2776	68 131	3.5	99 443	4.5	−2.77	1.11E+06	0.032
319.5182	72 375	1.5	103 664	1.5	−1.67	1.40E+07	0.533
319.8589	71 771	2.5	103 026	2.5	−1.51	2.02E+07	0.581
320.3243	68 131	3.5	99 341	3.5	−2.37	2.78E+06	0.183
321.3149	68 966	1.5	100 079	1.5	−3.15	4.62E+05	0.056
321.4008	70 635	2.5	101 740	3.5	−3.74	1.18E+05	0.006
322.0250	68 966	1.5	100 010	0.5	−2.78	1.07E+06	0.128
322.2422	68 131	3.5	99 155	4.5	−2.57	1.73E+06	0.077
323.6733	68 154	1.5	99 041	1.5	−2.61	1.55E+06	0.066
324.3358	68 736	2.5	99 559	2.5	−3.02	6.05E+05	0.024
325.8741	72 986	1.5	103 664	1.5	−2.84	9.27E+05	0.028
326.0705	70 707	1.5	101 366	2.5	−2.17	4.25E+06	0.129
326.1685	72 375	1.5	103 026	2.5	−2.82	9.55E+05	0.062
326.5761	70 635	2.5	101 247	2.5	−3.52	1.88E+05	0.019
326.6544	68 736	2.5	99 341	3.5	−1.67	1.33E+07	0.399
327.2246	70 707	1.5	101 258	1.5	−3.11	4.83E+05	0.021
327.3386	70 707	1.5	101 247	2.5	−2.70	1.25E+06	0.154
327.3516	70 707	1.5	101 246	0.5	−1.87	8.33E+06	0.764
327.6744	70 749	0.5	101 258	1.5	−2.12	4.76E+06	0.154
327.6759	70 635	2.5	101 145	3.5	−2.95	6.99E+05	0.056
327.8017	70 749	0.5	101 246	0.5	−2.31	3.06E+06	0.407
328.5283	68 131	3.5	98 561	2.5	−1.87	8.37E+06	0.517
328.7779	68 154	1.5	98 561	2.5	−3.87	8.27E+04	0.036
329.5460	68 131	3.5	98 467	3.5	−2.14	4.45E+06	0.249
329.8861	68 736	2.5	99 041	1.5	−1.44	2.22E+07	0.605
331.7045	70 707	1.5	100 845	0.5	−3.07	5.14E+05	0.022
332.1667	70 749	0.5	100 845	0.5	−1.62	1.47E+07	0.721
332.4053	68 966	1.5	99 041	1.5	−2.98	6.32E+05	0.060
332.7945	72 986	1.5	103 026	2.5	−1.26	3.38E+07	0.710
333.5773	71 771	2.5	101 740	3.5	−3.50	1.89E+05	0.029
333.7100	70 635	2.5	100 593	3.5	−2.05	5.33E+06	0.124
334.8505	70 635	2.5	100 491	1.5	−1.79	9.63E+06	0.233
335.0203	70 635	2.5	100 476	3.5	−3.09	4.86E+05	0.077
335.1901	68 736	2.5	98 561	2.5	−3.67	1.28E+05	0.028
335.3068	70 778	3.5	100 593	3.5	−3.34	2.75E+05	0.013
335.6522	70 707	1.5	100 491	1.5	−1.45	2.12E+07	0.583
335.9221	73 903	0.5	103 664	1.5	−1.57	1.60E+07	0.586
335.9920	70 635	2.5	100 390	2.5	−2.15	4.22E+06	0.178
336.1255	70 749	0.5	100 491	1.5	−2.20	3.71E+06	0.248
336.7992	70 707	1.5	100 390	2.5	−2.51	1.84E+06	0.084
337.6108	70 778	3.5	100 390	2.5	−3.69	1.19E+05	0.013
338.2669	70 778	3.5	100 332	4.5	−3.20	3.67E+05	0.096
339.1555	71 771	2.5	101 247	2.5	−3.41	2.23E+05	0.033
339.5382	70 635	2.5	100 079	1.5	−1.75	1.02E+07	0.573
340.2680	74 283	0.5	103 664	1.5	−2.50	1.80E+06	0.445
340.3625	70 707	1.5	100 079	1.5	−2.75	1.03E+06	0.053
340.4719	74 301	1.5	103 664	1.5	−3.68	1.23E+05	0.055
340.8491	70 749	0.5	100 079	1.5	−2.86	7.98E+05	0.068
341.1595	70 707	1.5	100 010	0.5	−1.88	7.59E+06	0.440

Table A.1. continued.

λ^a (nm)	Lower odd level^b		Upper 4d level^b		HFR+CPOL^c		
	E (cm^{-1})	J	E (cm^{-1})	J	log gf	gA (s^{-1})	CF
341.6483	70 749	0.5	100 010	0.5	−3.51	1.77E+05	0.011
345.6362	70 635	2.5	99 559	2.5	−1.45	2.02E+07	0.414
346.2577	72 375	1.5	101 247	2.5	−3.43	2.03E+05	0.027
346.4905	70 707	1.5	99 559	2.5	−2.25	3.17E+06	0.115
347.3494	70 778	3.5	99 559	2.5	−2.02	5.26E+06	0.125
348.0334	74 301	1.5	103 026	2.5	−2.64	1.27E+06	0.415
348.0883	71 771	2.5	100 491	1.5	−2.58	1.44E+06	0.209
348.2706	70 635	2.5	99 341	3.5	−3.72	1.06E+05	0.006
348.7608	70 778	3.5	99 443	4.5	−2.13	4.08E+06	0.122
349.3220	71 771	2.5	100 390	2.5	−3.39	2.21E+05	0.038
350.0101	70 778	3.5	99 341	3.5	−2.75	9.61E+05	0.116
351.9465	70 635	2.5	99 041	1.5	−1.85	7.70E+06	0.373
352.2540	72 986	1.5	101 366	2.5	−3.75	9.65E+04	0.020
352.3012	70 778	3.5	99 155	4.5	−2.98	5.71E+05	0.021
353.1567	71 771	2.5	100 079	1.5	−2.45	1.87E+06	0.260
353.3552	70 749	0.5	99 041	1.5	−3.98	5.59E+04	0.009
353.7344	72 986	1.5	101 247	2.5	−2.88	7.13E+05	0.079
353.7495	72 986	1.5	101 246	0.5	−3.08	4.44E+05	0.073
355.5737	72 375	1.5	100 491	1.5	−3.92	6.29E+04	0.026
356.8612	72 375	1.5	100 390	2.5	−2.97	5.60E+05	0.143
358.9066	70 707	1.5	98 561	2.5	−3.61	1.28E+05	0.010
359.1988	70 635	2.5	98 467	3.5	−2.61	1.29E+06	0.067
359.7584	71 771	2.5	99 559	2.5	−2.97	5.57E+05	0.065
359.8284	70 778	3.5	98 561	2.5	−1.24	3.01E+07	0.685
361.0496	70 778	3.5	98 467	3.5	−1.40	2.07E+07	0.446
361.7601	72 375	1.5	100 010	0.5	−3.40	2.04E+05	0.149
362.6134	71 771	2.5	99 341	3.5	−3.35	2.26E+05	0.022
363.4627	72 986	1.5	100 491	1.5	−3.73	9.59E+04	0.019
364.8080	72 986	1.5	100 390	2.5	−3.71	9.78E+04	0.026
366.6000	71 771	2.5	99 041	1.5	−3.99	5.08E+04	0.006
366.7136	76 402	2.5	103 664	1.5	−2.65	1.12E+06	0.020
368.7905	75 918	3.5	103 026	2.5	−2.33	2.30E+06	0.037
370.7754	74 283	0.5	101 246	0.5	−3.34	2.16E+05	0.216
374.4756	71 771	2.5	98 467	3.5	−3.45	1.68E+05	0.065
374.9122	72 375	1.5	99 041	1.5	−3.79	7.70E+04	0.041
375.5006	76 402	2.5	103 026	2.5	−3.01	4.68E+05	0.023
376.0069	73 903	0.5	100 491	1.5	−3.45	1.68E+05	0.101
376.2053	72 986	1.5	99 559	2.5	−3.12	3.60E+05	0.080
376.3696	74 283	0.5	100 845	0.5	−3.97	4.95E+04	0.062
381.4587	75 149	4.5	101 357	4.5	−3.79	7.50E+04	0.100
381.9278	73 903	0.5	100 079	1.5	−3.81	7.14E+04	0.072
387.1473	75 918	3.5	101 740	3.5	−3.38	1.82E+05	0.025
387.5554	74 283	0.5	100 079	1.5	−3.49	1.41E+05	0.197
388.5890	74 283	0.5	100 010	0.5	−3.86	6.01E+04	0.157
392.9771	75 918	3.5	101 357	4.5	−2.62	1.04E+06	0.151
394.5487	76 402	2.5	101 740	3.5	−1.57	1.15E+07	0.545
394.6811	75 918	3.5	101 247	2.5	−3.49	1.38E+05	0.026
397.6995	73 903	0.5	99 041	1.5	−3.29	2.20E+05	0.182
400.4618	76 402	2.5	101 366	2.5	−2.81	6.39E+05	0.234
402.3762	76 402	2.5	101 247	2.5	−1.75	7.35E+06	0.543
403.8052	74 283	0.5	99 041	1.5	−3.57	1.06E+05	0.131
404.0471	76 402	2.5	101 145	3.5	−2.48	1.34E+06	0.294
404.7172	75 918	3.5	100 619	4.5	−1.95	4.53E+06	0.474
405.1483	75 918	3.5	100 593	3.5	−2.36	1.76E+06	0.357
407.0812	75 918	3.5	100 476	3.5	−1.95	4.51E+06	0.596
408.5168	75 918	3.5	100 390	2.5	−3.50	1.28E+05	0.060
409.4777	75 918	3.5	100 332	4.5	−2.17	2.66E+06	0.462
413.2612	76 402	2.5	100 593	3.5	−2.35	1.75E+06	0.229

Table A.1. continued.

λ^a (nm)	Lower odd level^b		Upper 4d level^b		HFR+CPOL^c		
	E (cm^{-1})	J	E (cm^{-1})	J	log gf	gA (s^{-1})	CF
415.2724	76 402	2.5	100 476	3.5	−2.88	5.04E+05	0.168
416.7665	76 402	2.5	100 390	2.5	−1.92	4.61E+06	0.559
424.9559	75 918	3.5	99 443	4.5	−1.83	5.43E+06	0.394
426.8121	75 918	3.5	99 341	3.5	−1.65	8.29E+06	0.667
430.0280	75 722	5.5	98 969	5.5	−3.96	4.00E+04	0.044
430.2238	75 918	3.5	99 155	4.5	−2.46	1.26E+06	0.237
431.7079	76 402	2.5	99 559	2.5	−3.01	3.55E+05	0.145
435.8254	76 402	2.5	99 341	3.5	−3.23	2.07E+05	0.030
443.3420	75 918	3.5	98 467	3.5	−3.84	4.90E+04	0.015
456.1340	79 823	3.5	101 740	3.5	−3.02	3.04E+05	0.299
468.8767	79 823	3.5	101 145	3.5	−3.84	4.35E+04	0.185
481.3303	79 823	3.5	100 593	3.5	−3.51	8.85E+04	0.188
483.0646	79 924	4.5	100 619	4.5	−3.34	1.32E+05	0.165
489.8621	79 924	4.5	100 332	4.5	−3.59	7.05E+04	0.263
512.1791	79 924	4.5	99 443	4.5	−3.30	1.29E+05	0.095
512.2174	79 823	3.5	99 341	3.5	−3.47	8.73E+04	0.062
519.8509	79 924	4.5	99 155	4.5	−3.67	5.31E+04	0.038